Physical Sciences Publications   Physical Sciences

2012-06-13

Discovery Of Tev Gamma-Ray Emission Toward Supernova Remnant Snr G78.2+2.1

P. T. Reynolds
Cork Institute of Technology

Et. al.

Recommended Citation

Aliu, E. et al. (2013) 'DISCOVERY OF TeV GAMMA-RAY EMISSION TOWARD SUPERNOVA REMNANT SNR G78.2+2.1', The Astrophysical Journal, 770(2), p. 93. doi: 10.1088/0004-637X/770/2/93.

DISCOVERY OF TeV GAMMA-RAY EMISSION TOWARD SUPERNOVA REMNANT SNR G78.2+2.1

E. ALIU[1], S. ARCHAMBAULT[2], T. ARLEN[3], T. AUNE[3], M. BEILICKE[4], W. BENBOW[5], R. BIRD[6], A. BOUVIER[7], S. M. BRADBURY[8],
J. H. BUCKLEY[4], V. BUGAEV[4], K. BYRUM[9], A. CANNON[6], A. CESARINI[10], L. CIUPIK[11], E. COLLINS-HUGHES[6], M. P. CONNOLLY[10],
W. CUI[12], R. DICKHERBER[4], C. DUKE[13], J. DUMM[14], V. V. DWARKADAS[15], M. ERRANDO[1], S. FALCONE[16], S. FEDERICI[17,18],
Q. FENG[12], J. P. FINLEY[12], G. FINNEGAN[19], L. FORTSON[14], A. FURNISS[7], N. GALANTE[5], D. GALL[20], G. H. GILLANDERS[10],
S. GODAMBE[19], E. V. GOTTHELF[21], S. GRIFFIN[2], J. GRUBE[11], G. GYUK[11], D. HANNA[2], J. HOLDER[22], H. HUAN[23], G. HUGHES[17],
T. B. HUMENSKY[24], P. KAARET[20], N. KARLSSON[14], M. KERTZMAN[25], Y. KHASSEN[6], D. KIEDA[19], H. KRAWCZYNSKI[4],
F. KRENNRICH[26], M. J. LANG[10], K. LEE[4], A. S MADHAVAN[26], G. MAIER[17], P. MAJUMDAR[3,27], S. MCARTHUR[23], A. MCCANN[28],
J. MILLIS[29], P. MORIARTY[30], R. MUKHERJEE[1], T. NELSON[14], A. O'FAOLÁIN DE BHRÓITHE[6], R. A. ONG[3], M. ORR[26], A. N. OTTE[31],
D. PANDEL[32], N. PARK[23], J. S. PERKINS[33,34], M. POHL[17,18], A. POPKOW[3], H. PROKOPH[17], J. QUINN[6], K. RAGAN[2], L. C. REYES[35],
P. T. REYNOLDS[36], E. ROACHE[5], H. J. ROSE[8], J. RUPPEL[17,18], D. B. SAXON[22], M. SCHROEDTER[5], G. H. SEMBROSKI[12],
G. D. ŞENTÜRK[24], C. SKOLE[17], I. TELEZHINSKY[17,18], G. TEŠIĆ[2], M. THEILING[12], S. THIBADEAU[4], K. TSURUSAKI[20], J. TYLER[2],
A. VARLOTTA[12], V. V. VASSILIEV[3], S. VINCENT[17], S. P. WAKELY[23], J. E. WARD[4], T. C. WEEKES[5], A. WEINSTEIN[26],
T. WEISGARBER[23], R. WELSING[17], D. A. WILLIAMS[7], AND B. ZITZER[9]

[1] Department of Physics and Astronomy, Barnard College, Columbia University, NY 10027, USA
[2] Physics Department, McGill University, Montreal, QC H3A 2T8, Canada
[3] Department of Physics and Astronomy, University of California, Los Angeles, CA 90095, USA
[4] Department of Physics, Washington University, St. Louis, MO 63130, USA
[5] Fred Lawrence Whipple Observatory, Harvard-Smithsonian Center for Astrophysics, Amado, AZ 85645, USA
[6] School of Physics, University College Dublin, Belfield, Dublin 4, Ireland
[7] Santa Cruz Institute for Particle Physics and Department of Physics, University of California, Santa Cruz, CA 95064, USA
[8] School of Physics and Astronomy, University of Leeds, Leeds, LS2 9JT, UK
[9] Argonne National Laboratory, 9700 S. Cass Avenue, Argonne, IL 60439, USA
[10] School of Physics, National University of Ireland Galway, University Road, Galway, Ireland
[11] Astronomy Department, Adler Planetarium and Astronomy Museum, Chicago, IL 60605, USA
[12] Department of Physics, Purdue University, West Lafayette, IN 47907, USA
[13] Department of Physics, Grinnell College, Grinnell, IA 50112-1690, USA
[14] School of Physics and Astronomy, University of Minnesota, Minneapolis, MN 55455, USA
[15] Department of Astronomy and Astrophysics, University of Chicago, Chicago, IL 60637, USA
[16] Department of Astronomy and Astrophysics, 525 Davey Lab, Pennsylvania State University, University Park, PA 16802, USA
[17] DESY, Platanenallee 6, D-15738 Zeuthen, Germany
[18] Institute of Physics and Astronomy, University of Potsdam, D-14476 Potsdam-Golm, Germany
[19] Department of Physics and Astronomy, University of Utah, Salt Lake City, UT 84112, USA
[20] Department of Physics and Astronomy, University of Iowa, Van Allen Hall, Iowa City, IA 52242, USA
[21] Columbia Astrophysics Laboratory, Columbia University, New York, NY 10027, USA
[22] Department of Physics and Astronomy and the Bartol Research Institute, University of Delaware, Newark, DE 19716, USA
[23] Enrico Fermi Institute, University of Chicago, Chicago, IL 60637, USA
[24] Physics Department, Columbia University, New York, NY 10027, USA
[25] Department of Physics and Astronomy, DePauw University, Greencastle, IN 46135-0037, USA
[26] Department of Physics and Astronomy, Iowa State University, Ames, IA 50011, USA; amandajw@iastate.edu
[27] Saha Institute of Nuclear Physics, 1/AF Bidhannagar, Sector-1 Kolkata-700064, India
[28] Kavli Institute for Cosmological Physics, University of Chicago, Chicago, IL 60637, USA
[29] Department of Physics, Anderson University, 1100 East 5th Street, Anderson, IN 46012, USA
[30] Department of Life and Physical Sciences, Galway-Mayo Institute of Technology, Dublin Road, Galway, Ireland
[31] School of Physics and Center for Relativistic Astrophysics, Georgia Institute of Technology, 837 State Street NW, Atlanta, GA 30332-0430, USA
[32] Department of Physics, Grand Valley State University, Allendale, MI 49401, USA
[33] CRESST and Astroparticle Physics Laboratory NASA/GSFC, Greenbelt, MD 20771, USA
[34] University of Maryland, Baltimore County, 1000 Hilltop Circle, Baltimore, MD 21250, USA
[35] Physics Department, California Polytechnic State University, San Luis Obispo, CA 94307, USA
[36] Department of Applied Physics and Instrumentation, Cork Institute of Technology, Bishopstown, Cork, Ireland

ABSTRACT

We report the discovery of an unidentified, extended source of very-high-energy gamma-ray emission, VER J2019+407, within the radio shell of the supernova remnant SNR G78.2+2.1, using 21.4 hr of data taken by the VERITAS gamma-ray observatory in 2009. These data confirm the preliminary indications of gamma-ray emission previously seen in a two-year (2007–2009) blind survey of the Cygnus region by VERITAS. VER J2019+407, which is detected at a post-trials significance of 7.5 standard deviations in the 2009 data, is localized to the northwestern rim of the remnant in a region of enhanced radio and X-ray emission. It has an intrinsic extent of $0°.23 \pm 0°.03_{stat}{}^{+0°.04}_{-0°.02sys}$ and its spectrum is well-characterized by a differential power law ($dN/dE = N_0 \times (E/\mathrm{TeV})^{-\Gamma}$) with a photon index of $\Gamma = 2.37 \pm 0.14_{stat} \pm 0.20_{sys}$ and a flux normalization of $N_0 = 1.5 \pm 0.2_{stat} \pm 0.4_{sys} \times 10^{-12}$ photon $\mathrm{TeV}^{-1}\,\mathrm{cm}^{-2}\,\mathrm{s}^{-1}$. This yields an integral flux of $5.2 \pm 0.8_{stat} \pm 1.4_{sys} \times 10^{-12}$ photon $\mathrm{cm}^{-2}\,\mathrm{s}^{-1}$ above 320 GeV, corresponding to 3.7% of the Crab Nebula flux. We consider the relationship of the TeV gamma-ray emission with the GeV gamma-ray emission seen from SNR G78.2+2.1 as well as that seen from a nearby cocoon of freshly accelerated cosmic rays.

Multiple scenarios are considered as possible origins for the TeV gamma-ray emission, including hadronic particle acceleration at the SNR shock.

Key words: acceleration of particles – cosmic rays – gamma rays: general – ISM: supernova remnants

1. INTRODUCTION

The stereoscopic imaging atmospheric Cherenkov telescope array VERITAS completed a two-year survey of the Cygnus region of the Galactic Plane in very high energy (VHE) gamma rays (Weinstein et al. 2009). The survey covered the area between Galactic longitudes $67°$ and $82°$ and Galactic latitudes $-1°$ and $4°$, a region chosen because it contains both a high density of material and a significant population of potential VHE gamma-ray emitters, including a number of pulsar wind nebulae (PWNe) and supernova remnants (SNRs). As acceleration of either electrons or nuclei above 1 TeV within these stellar remnants can also generate gamma-ray emission, detection of gamma rays from these objects may provide insight into the nature of both the acceleration process within the remnant and the nature of the accelerated population of particles (Blandford & Eichler 1987; Ellison & Reynolds 1991; Drury et al. 1994; Ellison et al. 2007). Relativistic electrons can produce gamma rays via both non-thermal bremsstrahlung and inverse-Compton (IC) scattering off nearby optical, IR, or microwave photons. Protons and heavier atomic nuclei generate gamma rays via the decay of neutral pions produced by their interaction with interstellar material. Identifying gamma-ray emission from SNRs that is produced by pion decay could provide insight into the origin of Galactic cosmic rays by providing evidence that SNRs are sites of hadronic cosmic ray acceleration within the Galaxy.

While the initial survey yielded no clear new source detections, the blind search suggested possible VHE gamma-ray emission at several locations, most notably in the vicinity of the SNR G78.2+2.1 (γ-Cygni). SNR G78.2+2.1 is a $\sim1°$ diameter SNR ~1.7 kpc distant, with a shell-like radio and X-ray structure (Higgs et al. 1977; Lozinskaya et al. 2000). It is considered young to middle-aged at ~7000 yr (Higgs et al. 1977; Landecker et al. 1980; Lozinskaya et al. 2000) and in an early phase of adiabatic expansion into a medium of fairly low density (Lozinskaya et al. 2000). Gosachinskij (2001) also identifies a slowly expanding H I shell immediately surrounding the radio shell. Lozinskaya et al. (2000) suggest this shell was created by the progenitor stellar wind.

Most of the radio and X-ray emission lies in distinct northern and southern features (Zhang et al. 1997; Uchiyama et al. 2002). The northern region is characterized by enhanced thermal X-ray emission, suggestive of shocked gas (Uchiyama et al. 2002), as well as strong optical emission with sulfur lines (Mavromatakis 2003). However, it evinces little to no CO emission (Ladouceur & Pineault 2008). The gamma-ray satellite *Fermi* sees diffuse gamma-ray emission above 10 GeV from the entire remnant (Lande et al. 2012) and has discovered a gamma-ray pulsar, PSR J2021+4026, at the center of the remnant (Abdo et al. 2010a, 2010b). This pulsar, which has a spectral cutoff of 3.0 GeV, also has a low luminosity (1.1×10^{35} erg s^{-1}) and a spin-down age (76.8 kyr) much greater than the estimated age of SNR G78.2+2.1. Trepl et al. (2010) argue, however, that PSR J2021+4026 was likely born with something close to its current spin period, in which case its spin-down age is not indicative of its actual age. It therefore remains plausible that

PSR J2021+4026 is the remnant of SNR G78.2+2.1's progenitor star (Trepl et al. 2010). Except where otherwise noted, all GeV and TeV sources are considered to be at a distance of 1.7 kpc, the estimated distance of SNR G78.2+2.1 (Higgs et al. 1977; Lozinskaya et al. 2000).

Subsequent to the completion of the VERITAS Cygnus region survey, follow-up observations were taken of the VHE gamma-ray source candidate near SNR G78.2+2.1. Based on those further observations, we report here the discovery of an extended, unidentified source of VHE gamma rays that lies within an area of enhanced radio emission along the northwestern shell of SNR G78.2+2.1. The observational details are described in Section 2; the analysis and results are presented in Sections 3 and 4, respectively. We discuss the nature of the TeV gamma-ray emission in Section 5.

2. OBSERVATIONS

The VERITAS Observatory consists of an array of four imaging atmospheric Cherenkov telescopes, located at the Fred Lawrence Whipple Observatory in southern Arizona (Holder et al. 2008). Each telescope is equipped with a $3°.5$ field-of-view (FOV), 499 pixel photomultiplier tube camera. The array is run in a coincident mode, requiring a minimum of two out of four telescopes to trigger in order for an event to be recorded. Data included in this paper were taken with an upgraded array configuration that has improved sensitivity and gamma-ray point-spread function (PSF; Perkins et al. 2009) relative to that used during the Cygnus region survey. This configuration has $\sim15\%$–25% energy resolution between 100 GeV and 30 TeV and a 5σ (standard deviation above background) point source sensitivity of 1% of the Crab Nebula flux above 300 GeV in less than 30 hr of observation at zenith angles less than $30°$.

The observations under discussion were motivated by, but do not include, data from the VERITAS Cygnus region survey (Weinstein et al. 2009). The initial two-year survey covered the area of the remnant with an effective exposure time of ~30 hr and showed evidence of an extended gamma-ray excess. The approximate location of the survey excess was re-observed with a set of dedicated pointings during 2009 September–November, for a total live-time of 18.6 hr. These observations were performed in "wobble" mode, with the center of the VERITAS FOV offset by $0°.6$ from the target position (R.A. $20^h19^m48^s$, decl. $+40°54'00''$). The zenith angle was restricted to $10°$–$30°$ for these observations. Approximately 10% of the data were taken at a time when three out of the four VERITAS telescopes were operational; the remaining 90% was taken with the full array.

3. ANALYSIS

Images from these data are calibrated according to the standard procedure described in Cogan et al. (2008) and cleaned using the procedure described in Daniel et al. (2008). After calibration, the primary photon direction is calculated via stereoscopic reconstruction based on the intersection of image primary axes. To ensure that the primary photon direction and energy can be well-reconstructed, an initial event selection is
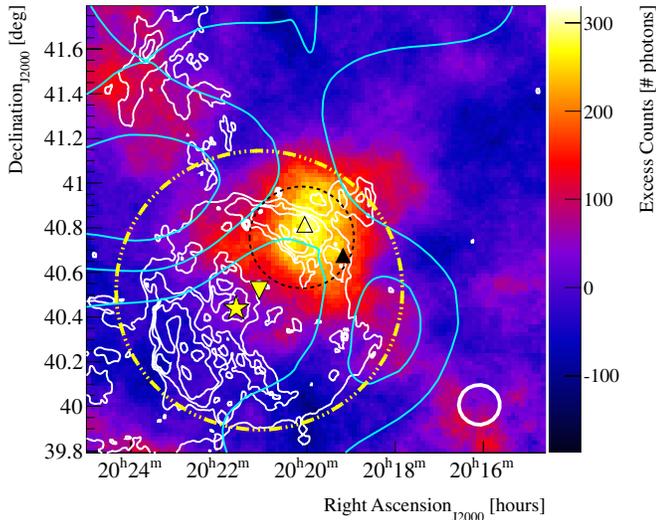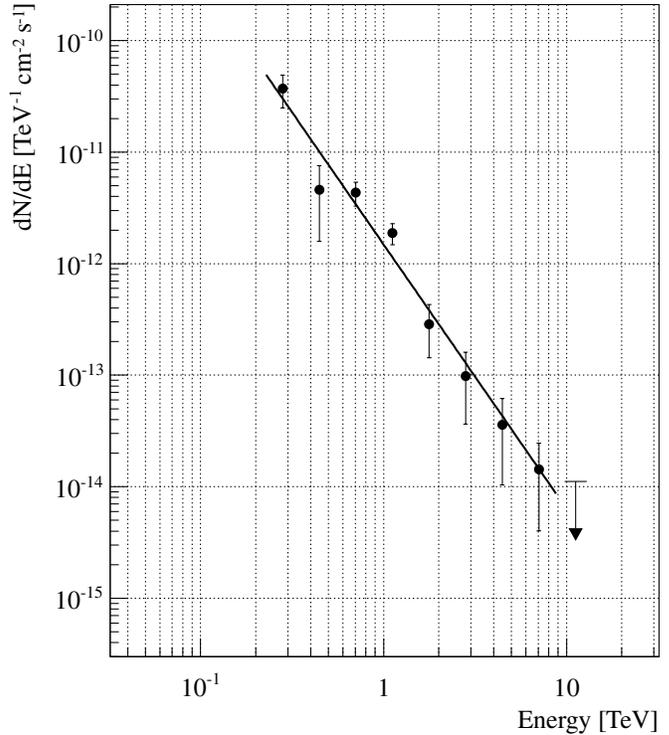
Figure 1. Background-subtracted gamma-ray counts map of SNR G78.2+2.1 showing the VERITAS detection of VER J2019+407 and its fitted extent (black dashed circle). The supernova remnant is delineated by CGPS 1420 MHz continuum radio contours at brightness temperatures of 23.6 K, 33.0 K, 39.6 K, 50 K, and 100 K (white; Taylor et al. 2003); the star shows the location of the central gamma-ray pulsar PSR J2021+4026. The inverted triangle and dot-dashed circle (yellow) show the fitted centroid and extent of the emission detected by *Fermi* above 10 GeV. The open and filled triangles (black) show the positions of *Fermi* catalog sources 1FGL J2020.0+4049 and 2FGL J2019.1+4040 which have been subsumed into the extended GeV emission from the entire remnant. The 0.16, 0.24, and 0.32 photons bin^{-1} contours of the *Fermi* detection of the Cygnus cocoon are shown in cyan. The white circle (bottom right corner) indicates the 68% containment size of the VERITAS gamma-ray PSF for this analysis.


Figure 2. Spectrum of VER J2019+407, derived from four-telescope data only. Points are the VERITAS spectrum, while the arrow indicates the upper limit on emission at 11 TeV. The solid line shows a power-law fit with a spectral index of $\Gamma = 2.37 \pm 0.14_{\text{stat}} \pm 0.20_{\text{sys}}$ and a flux normalization of $N_0 = 1.5 \pm 0.2_{\text{stat}} \pm 0.4_{\text{sys}} \times 10^{-12}$ photon $\text{TeV}^{-1}\,\text{cm}^{-2}\,\text{s}^{-1}$.

applied, requiring that events have three images passing the following criteria: more than four pixels per image, an image centroid no more than 1°.43 from the camera center, and a total integrated charge per image of at least 70 photoelectrons.

Calibrated images are described in terms of a second-moment parameterization (Hillas 1985). Cosmic-ray background is rejected using selection criteria applied to two composite parameters based on these moments: mean-scaled length (MSL) and mean-scaled width (MSW; Aharonian et al. 1997). We impose the requirements $0.05 < \text{MSL} < 1.25$ and $0.05 < \text{MSW} < 1.10$; in addition, we require the angle between the reconstructed gamma-ray arrival direction and the source position to be less than 0°.23. The chosen background-rejection criteria are optimized for moderate-strength (∼5% of the Crab nebula flux) extended sources. Together with the image quality requirements they impose an energy threshold for this measurement of 320 GeV.

To minimize the number of independent search elements, our search is restricted to a pre-defined circular region with radius 0°.25 centered on the target position. In the imaging analysis and source morphology studies the ring background model (Aharonian et al. 2005) is used to estimate the residual cosmic ray background; the reflected-region model (Aharonian et al. 2001) is used when extracting the spectrum. We also excluded from the background estimation circular regions with radius 0°.3 around four bright stars in the FOV (γ Cygni, P Cygni, 40 Cygni, and HIP100069) as well as two overlapping circular 0°.4 radius regions used to approximate the profile of the excess seen in the VERITAS survey data (Weinstein et al. 2009, 2011). All results reported here have been verified by an independent calibration and analysis chain.

4. RESULTS

Figure 1 displays the background-subtracted, acceptance-corrected TeV image of the region of SNR G78.2+2.1. A clear signal with 319 ± 39 net counts is detected at the location of the northern rim of the remnant. This signal is significant at the 7.5σ level after accounting for all test points in the pre-defined 0°.25 search region. Figure 1 also shows the locations of the gamma-ray pulsar PSR J2021+4026 (1FGL J2021.5+4026), ∼0°.5 from VER J2019+407 at the center of the SNR, and the centroid of the emission from the remnant seen by *Fermi* above 10 GeV.

The morphology of VER J2019+407 is derived from a binned extended maximum-likelihood fit to the counts map before background subtraction. The cosmic ray component is modeled as an exposure-modulated flat background and the source by a symmetric two-dimensional Gaussian convolved with the VERITAS PSF (68% containment radius of 0°.09, derived from an identically processed observation of the Crab Nebula). We find a fitted extension of $0°.23 \pm 0°.03_{\text{stat}}{}^{+0°.04}_{-0°.02\text{sys}}$. The fitted centroid coordinates are R.A. $20^h20^m04^s.8$, decl. $+40°45'36''$ (J2000); however, we maintain the identifier VER J2019+407 for the source, which was originally assigned on the basis of a preliminary centroid estimation. The statistical uncertainty in this location is 0°.03, with a combined systematic uncertainty in the position, due to the telescope pointing error and systematic errors of the fit itself, of 0°.018.

Figure 2 shows the spectrum derived from the reconstructed gamma-ray events within 0°.24 from the center of the search region; runs where only three of four telescopes were operational have been excluded from this sample. The threshold for the spectral analysis is 320 GeV and the energy resolution is 15% at

3
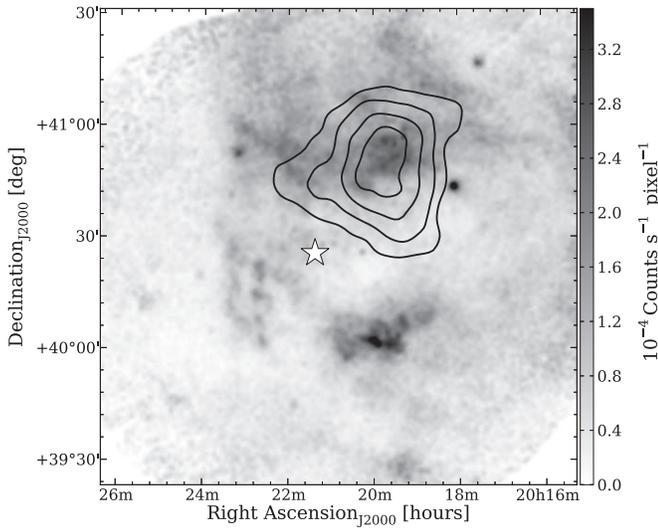
Figure 3. *ROSAT* PSPC X-ray view of SNR G78.2+2.1 between 1 and 2 keV. The VER J2019+407 smoothed photon excess contours (100, 150, 210, and 260 photons) are superimposed. The image is composed of a mosaic of six exposure- and vignette-corrected overlapping observations, smoothed using a 5 × 5 pixel boxcar filter. The lower energy bound was selected to reject the background flux from the Galactic Plane. The location of the gamma-ray pulsar PSR J2021+4026 is marked with a white star.


Figure 4. ASCA X-ray view of G78.2+2.1 between 1 and 3 keV, overlaid with the VER J2019+407 smoothed photon excess contours (100, 150, 210, and 260 photons). The region used to extract a spectrum and the corresponding background region are indicated by white solid and dashed ellipses, respectively. A white star marks the position of PSR J2021+4026.

1 TeV. The photon spectrum is fit well ($\chi^2/\text{dof} = 8.76/6$) by a differential power law in energy, $dN/dE = N_0 \times (E/\text{TeV})^{-\Gamma}$, between 320 GeV and 10 TeV, with a photon index of $2.37 \pm 0.14_{\text{stat}} \pm 0.20_{\text{sys}}$ and a flux normalization at 1 TeV of $N_0 = 1.5 \pm 0.2_{\text{stat}} \pm 0.4_{\text{sys}} \times 10^{-12}$ photon TeV^{-1} cm^{-2} s^{-1}. The integral flux above 320 GeV ($5.2 \pm 0.8_{\text{stat}} \pm 1.4_{\text{sys}} \times 10^{-12}$ photon cm^{-2} s^{-1}) corresponds to 3.7% of the Crab Nebula flux above that energy. No other significant TeV source is found in the maps.

4.1. X-Ray Observations

Figure 3 presents an exposure-corrected *ROSAT* PSPC 1–2 keV image of SNR G78.2+2.1 generated from archival data (see Brazier et al. 1996 for observational details). The TeV gamma-ray emission overlaps a region of enhanced X-ray emission coincident with the bright radio arcs associated with the northern rim of the SNR shell. As the highly absorbing column to the remnant screens out most source photons below ~1 keV, we excluded all photons below this energy to suppress background. Several bright X-ray sources are associated with known stars and have been identified in previous work, but none of these overlap the VHE gamma-ray-emitting region (Becker et al. 2004; Weisskopf et al. 2006).

To better study the enhanced X-ray emission overlapping the TeV contours, we also re-analyzed the data from ASCA Sequence #25010000 previously studied by Uchiyama et al. (2002). Figure 4 shows the 0.7–3.0 keV exposure-corrected X-ray map, generated by co-adding data from the two gas imaging spectrometers. The image is consistent with that seen by *ROSAT*. We extracted source and background spectra from the two $12' \times 24'$ elliptical regions displayed in Figure 4 and generated count-weighted response files appropriate for diffuse emission. The source region, centered on coordinates R.A. $20^h20^m17^s$, decl. $+40°45'41''$ (J2000) and oriented with position angle 60°, contains the bulk of the X-ray emission located within the VERITAS contours. The background ellipse, centered at R.A. $20^h19^m38^s$, decl. $+40°27'02''$ (J2000) with position
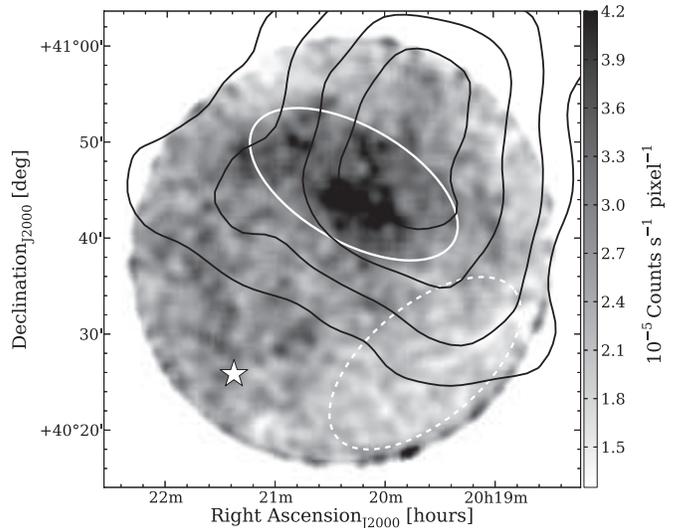
angle 130°, is placed where the X-ray emission is evidently at background level in the *ROSAT* image. The source spectrum was grouped with a minimum of 20 counts per channel and fitted in the 0.7–3.0 keV range using the XSPEC software package. The spectra are evidently soft with few net counts above ~3 keV after background subtraction. A significant line feature is found at 1.9 keV; we do not, however, find any evidence for the strong Ne line feature at ≃0.9 keV reported by Uchiyama et al. (2002).

We modeled the X-ray spectrum using an absorbed Raymond–Smith thermal plasma model (see Figure 5). This provides an adequate fit with $\chi^2/\text{dof} = 40.8/44$. The best-fitted temperature is $kT = 0.57 \pm 0.14$ keV. Si is overabundant by a factor of $2.0^{+1.8}_{-1.2}$ relative to solar. The column density is $N_H = (3.7 \pm 2.0) \times 10^{21}$ cm^{-2} and the normalization is $N = 1.8 \times 10^{-3}$ cm^{-5}. The absorption-corrected flux for this model is found to be 6.0×10^{-12} erg cm^{-2} s^{-1} in the 0.5–8.0 keV band. We also considered that the plasma behind a shock expanding in a low-density medium might not have had time to reach ionization equilibrium given the assumed SNR lifetime, in which case the spectrum would be better modeled by a non-equilibrium ionization (NEI) model. We attempted to fit the ASCA spectrum with an absorbed NEI model, the "vgnei" model of XSPEC, but were unable to obtain good constraints on the fitted parameters.

We also attempted to constrain the flux of any possible power-law component in the spectrum by adding a power-law with photon index fixed to 2.0 and then varying the power-law normalization until the χ^2 increased by 2.7 (90% confidence level) relative to the best fitted model with no power-law component. We place an upper limit on the flux of a power-law component of 1.9×10^{-12} erg cm^{-2} s^{-1} in the 0.5–8.0 keV band.

We note that our result differs significantly from that given in Uchiyama et al. (2002). While we have chosen a source region similar to their "R1" source region, we find that our fits to the ASCA spectrum require neither an additional power-law component nor a large Ne IX line feature. The discrepancy seems to be caused by the choice of background region. We selected a background region that was as close as possible to the source, in
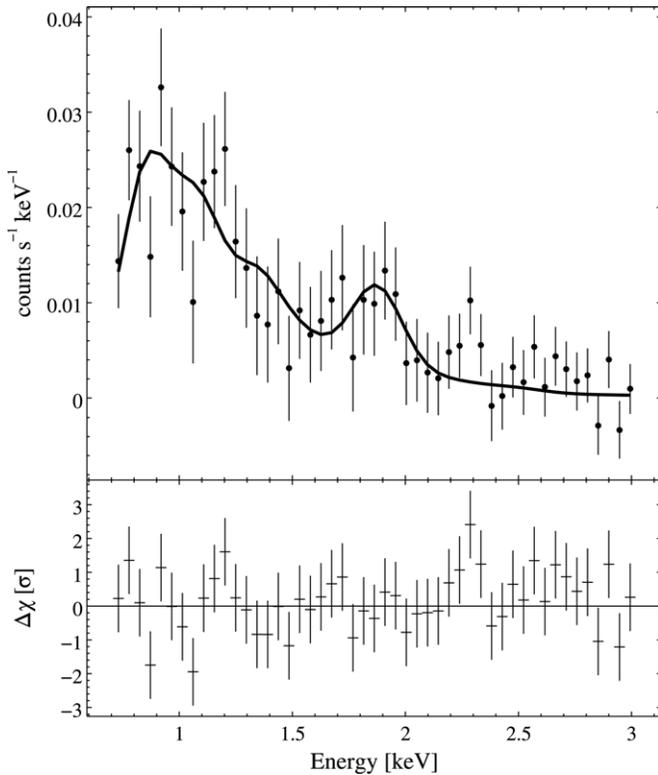
Figure 5. Top panel: ASCA X-ray spectrum of the region of enhanced X-ray emission coincident with VER J2019+407, as shown in Figure 4. The solid line shows the fit of a Raymond–Smith thermal plasma model with parameters as given in the text. We identify the line at 1.9 keV as due to Si. Bottom panel—$\Delta\chi$ residuals (residual divided by the statistical error) for the best-fit model.

order to account for the large variance in the Galactic emission in this part of the plane. Uchiyama et al. (2002) considered four nearby ASCA pointings and chose the one with the least source contamination, ~ 3.5 from the center of the "R1" region. A choice of background region similar to Uchiyama's allows us to reproduce the previously reported nonthermal component and spectral features.

5. DISCUSSION

We have discovered a spatially extended source of VHE gamma-ray emission, VER J2019+407, located on the north-west rim of the shell-type SNR G78.2+2.1. The TeV gamma-ray emission is coincident with the leading edge of a prominent arc-shaped radio continuum feature along the SNR rim (Figure 1) and with a region of enhanced X-ray emission that we identify as thermal in origin (Figures 3–5). VER J2019+407 lies near the inner edge of a slowly expanding H I shell immediately surrounding the radio shell identified in 21 cm line observations (Gosachinskij 2001); it also lies near a region of bright [S II] optical line emission within the SNR that is identified as shock-heated gas based on the [S II]/Hα line ratio (Mavromatakis 2003). There are also two GeV sources associated with SNR G78.2+2.1. One is a pulsar, 1FGL J2021.5+4026, located at the center of the remnant (Abdo et al. 2010a, 2010b). The other is an extended source candidate reported above 10 GeV by *Fermi* (Lande et al. 2012). A point source co-located with VER J2019+407 was previously reported in the first and second *Fermi* catalogs, but Lande et al. (2012) conclude that it was an artifact of failing to model the extended source above 10 GeV rather than a separate source. Between

G78.2+2.1 and the Cyg OB2 association (roughly 2°4 away) lies a 50 parsec-wide area of 1–100 GeV gamma-ray emission, detected by *Fermi*, that has been interpreted as a cocoon of freshly accelerated cosmic rays (Ackermann et al. 2011).

The TeV gamma-ray emission and the features observed in the X-ray, optical, and radio continuum can be most simply related to the presence of shocks at the interaction of the supernova ejecta and the surrounding medium. SNR G78.2+2.1 has a relatively low interior density and, as previously noted, appears to be surrounded by a dense H I shell (Gosachinskij 2001). Lozinskaya et al. (2000) suggest that this H I shell was created by the progenitor stellar wind as it swept up the ambient medium. The interaction of the supernova shock with the H I shell might drive a shock into the dense shell and a reflected shock back into the cavity. Emission arising from these shocks would then account for the observed [S II] lines, enhanced thermal X-rays, and strong radio continuum emission near VER J2019+407.

Shocks can produce TeV gamma-ray emission via either IC scattering of accelerated electrons or hadronic interactions of accelerated nuclei. High-energy electrons capable of producing TeV photons via IC scattering should also produce X-ray synchrotron radiation detectable as a non-thermal power-law in the X-ray spectrum. While our analysis of the ASCA X-ray spectrum shows no evidence for a non-thermal component, the upper limit on this component is not yet strong enough to rule out IC scattering as the source of the TeV, if not the GeV, gamma-ray emission. Deeper X-ray observations of VER J2019+407 should provide better constraints.

The flux of TeV photons from hadronic processes depends on the energy available for shock acceleration and the density of the target material. One of the prerequisites of this scenario is that the necessary density of target material, as inferred from the gamma-ray flux, be consistent with that estimated from measurements at other wavelengths. Equation (9) in Drury et al. (1994) gives (on the assumption that the spectrum of the charged particles is a power law with index of -2) the expected gamma-ray flux above a given threshold energy as a function of the threshold energy E, the fraction θ of the SN kinetic energy E_{SN} converted to cosmic rays, the distance d of the SNR, and the density n of the target material,

$$F(>E) \approx 9 \times 10^{-11}\theta \left(\frac{E}{1\,\mathrm{TeV}}\right)^{-1.1} \left(\frac{E_{\mathrm{SN}}}{10^{51}\,\mathrm{erg}}\right)$$
$$\times \left(\frac{d}{1\,\mathrm{kpc}}\right)^{-2} \left(\frac{n}{1\,\mathrm{cm}^{-3}}\right) \mathrm{cm}^{-2}\,\mathrm{s}^{-1}. \qquad (1)$$

For $E = 320$ GeV, $d = 1.7$ kpc, $\theta \sim 0.1$ as expected for a remnant in the early Sedov phase, and assuming $E_{\mathrm{SN}} = 10^{51}$ erg, which is consistent with estimates derived from optical data (Mavromatakis 2003), we find that a density of 0.5 cm^{-3} is required to produce the observed TeV flux. However, this equation is for the total flux integrated over the whole spherical shell of a SNR. The gamma-ray emission from VER J2019+407 is confined to a relatively small portion of the SNR shell. Thus, it is likely that only a fraction of the SN blast wave participates in the shock acceleration producing the TeV gamma-ray emission. Assuming an isotropic explosion, we account for this by scaling E_{SN} by the ratio of the surface area covered by VER J2019+407 to the total surface area of the remnant. Using the fitted 95% (68%) containment radius of the TeV gamma-ray emission gives a correction factor of 0.5 (0.14). Once uncertainties in the source extension, integral flux, and SNR distance are also taken into

account, the average density required to produce the observed TeV flux above 320 GeV increases to 1.0–5.5 cm^{-3}.

We find these densities consistent with our knowledge of the region from other wavelengths. Given that no significant CO emission is detected in this area of the remnant, any target material must be atomic rather than molecular, with the necessary high density perhaps arising in the swept-up H I shell. Gosachinskij (2001) estimated a gas density of 2.5 cm^{-3} in the H I shell surrounding the remnant, consistent with the range of densities derived from the TeV data. Optical data also shed some light on densities in the vicinity of VER J2019+407. Mavromatakis gives the ratio of [S II] λ6716 to [S II] λ6731 line fluxes at multiple locations within G78.2+2.1, one of which is close to (although not precisely coincident with) VER J2019+407. All of these ratios are close to one, and, within a plausible range of temperatures, imply post-shock densities on the order of a few 100 cm^{-3}. Mavromatakis infers these densities to be arising behind a radiative shock and estimates a primary shock velocity of $\sim$750 km s^{-1}, consistent with that inferred from an X-ray temperature of 0.57 keV. He deduces pre-shock cloud densities on the order of $\sim$20 cm^{-3}, which are not unreasonable given the average densities inferred here from the gamma-ray flux. The shock velocities inferred from the optical and X-ray data, however, are too low for the forward shock to accelerate particles to TeV energies at the present time. Any hadronic TeV gamma-ray emission would have to arise from particles accelerated during an earlier epoch that are only now interacting with the shell.

The limited angular extent of the TeV gamma-ray emission also raises questions. If we view the SN blastwave as expanding in the low-density bubble blown by the progenitor stellar wind until it reaches the much higher-density cavity wall, why should the interaction favor one portion of the cavity wall over the others? Asymmetries in the shock propagation, variations in the density of the cavity wall, or the former presence of a cloud (now evaporated by the shock) within the low density region could provide an explanation, as could the strength and orientation of the ambient magnetic field relative to the local shock velocity (Ellison et al. 2007). Given the more symmetric and diffuse GeV gamma-ray emission seen from the remnant, asymmetric diffusion of accelerated particles out of the remnant might also play a role, as the highest-energy particles would be the first to escape. However, at this stage there is no clear evidence for or against any of these possibilities.

In these scenarios, SNR G78.2+2.1 could be responsible for some or all of the freshly accelerated cosmic rays within the cocoon detected by *Fermi*. However, the results shown here cannot be used to draw strong conclusions about the cocoon's relationship to SNR G78.2+2.1 or to set a meaningful upper limit on cocoon emission above 300 GeV. The cocoon contours from Ackermann et al. (2011) were derived from an analysis where 1FGL J2020.0+4049, which is no longer considered an independent source, was included as part of the background model. Since this would artificially reduce the intensity of the GeV gamma-ray emission seen near VER J2019+407, the Ackermann et al. (2011) contours provide a spatial reference only and should not be used to judge the relationship of the cocoon to VER J2019+407. Moreover, gamma-ray emission on the scale of the cocoon (roughly 4 deg^2) cannot be detected with VERITAS using the ring-background estimation method, which will cause the source to self-subtract. Analysis techniques better adapted to highly extended sources, combined with further data taken in alternative observation modes, will be required to

confirm the presence or absence of cocoon emission and make a definitive statement about SNR G78.2+2.1's role in feeding the cocoon.

VER J2019+407 bears some similarity to other well known TeV sources. H.E.S.S. observations of the shell-type SNR RCW 86 have revealed the presence of VHE gamma rays suggestive of a shell-type morphology (Aharonian et al. 2009). Berezhko et al. (2009) have explained the TeV gamma-ray emission from RX J0852.0−4622 as arising from hadronic emission in a wind-bubble scenario, similar in many aspects to the scenario proposed here.

Other explanations of VER J2019+407 are also possible. Nearly half of Galactic TeV sources are identified with PWNe. TeV PWNe are typically extended sources energized by electrons accelerated in the pulsar wind. Because the lifetimes of the electrons can be long, the electrons can diffuse over large distances from the pulsar and the centroid of the TeV gamma-ray emission is often offset from the pulsar (Hessels et al. 2008). On the one hand, the luminosity of VER J2019+407 in the 1–10 TeV band—2.5×10^{33} erg s^{-1} assuming a distance of 1.7 kpc—is 2% of the spin-down power of PSR J2021+4026, a value within the range seen for PWNe. On the other hand, Hessels et al. (2008) examined the offsets between TeV gamma-ray emission and pulsar location for 21 TeV sources, and the pulsar, while offset from the centroid of the TeV gamma-ray emission, generally lies well within the angular extent of the TeV source. In the single case for which the angular offset is significantly larger than the angular size of the TeV source—PSR J1702−4128/HESS J1702−420– inspection of the TeV image shows TeV emission at the pulsar location (Aharonian et al. 2008). By contrast, the offset between PSR J2021+4026 and VER J2019+407 is several times larger than the angular size of VER J2019+407, and we detect no TeV gamma-ray emission either at the location of PSR J2021+4026 or in the intervening region between PSR J2021+4026 and the TeV source.

Finally, it is possible that VER J2019+407 is the PWN of an unknown pulsar in the line-of-sight toward SNR G78.2+2.1. This scenario could explain the GeV and radio continuum emission, but would ascribe the location of VER J2019+407 near the [S II] line emission and the enhanced thermal X-ray emission within SNR G78.2+2.1 to chance superposition. Such a scenario cannot be excluded at the current time, but could be tested by a sensitive search for the PWN in the X-ray band and also by radio or X-ray searches for the putative pulsar.

In summary, we have detected gamma-ray emission from a region of enhanced radio, optical line, and X-ray emission in the northwestern shell of SNR G78.2+2.1. The extended TeV source overlaps with GeV gamma-ray emission from the remnant but is notably offset from the gamma-ray pulsar PSR J2021+4026 which lies outside the 99% confidence contour of VER J2019+407. It seems most probable that VER J2019+407 arises from particles (either hadronic or leptonic) accelerated within the SNR shock, although we cannot yet rule out the possibility of a line-of-sight coincidence between the remnant and an un-associated PWN. Deeper high energy observations are needed to better constrain possible emission models.

REFERENCES

Abdo, A. A., Ackermann, M., Ajello, M., et al. 2010a, ApJS, 187, 460
Abdo, A. A., Ackermann, M., Ajello, M., et al. 2010b, ApJS, 188, 405
Ackermann, M., Ajello, M., Allafort, A., et al. 2011, Sci, 334, 1103
Aharonian, F. A., Akhperjanian, A. G., Aye, K.-M., et al. 2005, A&A, 430, 865
Aharonian, F. A., Akhperjanian, A. G., Barres de Almeida, U., et al. 2008, A&A, 477, 353
Aharonian, F. A., Akhperjanian, A. G., Barres de Almeida, U., et al. 2009, ApJ, 692, 1500
Aharonian, F. A., Akhperjanian, A., Barrio, J., et al. 2001, A&A, 370, 112
Aharonian, F. A., Hofmann, W., Konopelko, A. K., & Völk, H. J. 1997, APh, 6, 343
Becker, W., Weisskopf, M., Arzoumanian, Z., et al. 2004, ApJ, 615, 897
Berezhko, E. G., Puhlhofer, G., & Völk, H. J. 2009, A&A, 505, 641
Blandford, R., & Eichler, D. 1987, PhR, 154, 1
Brazier, K. T. S., Kanbach, G., Carramiñana, A., Guichard, J., & Merck, M. 1996, MNRAS, 281, 1033
Cogan, P., Acciari, V. A., Amini, R., et al. 2008, in Proc. 30th Int. Cosmic Ray Conf., Vol. 3, ed. R. Caballero, J. C. D'Olivo, G. Median-Tanco, L. Nellen, F. A. Sánchez, & J. F. Valdés-Galicia (Mexico City, Mexico: Universidad Nacional Autónoma de México), 1385
Daniel, M. K., Acciari, V. A., Amini, R., et al. 2008, in Proc. 30th Int. Cosmic Ray Conf., Vol. 3, ed. R. Caballero, J. C. D'Olivo, G. Median-Tanco, L. Nellen, F. A. Sánchez, & J. F. Valdés-Galicia (Mexico City, Mexico: Universidad Nacional Autónoma de México), 1325
Drury, L. O'C., Aharonian, F. A., & Völk, H. J. 1994, A&A, 287, 959
Ellison, D. C., Patnaude, D. J., Slane, P., Blasi, P., & Gabici, S. 2007, ApJ, 661, 879
Ellison, D. C., & Reynolds, S. P. 1991, ApJ, 382, 242
Gosachinskij, I. V. 2001, AstL, 27, 233
Hessels, J. W. T., Nice, D. J., Gaensler, B. M., et al. 2008, ApJL, 682, L41
Higgs, L. A., Landecker, T. L., & Roger, R. S. 1977, AJ, 82, 718
Hillas, A. M. 1985, in Proc. 19th Int. Cosmic Ray Conf., Vol. 3, ed. F. C. Jones, 445
Holder, J., Acciari, V. A., Aliu, E., et al. 2008, in AIP Conf. Proc. 1085, Proc. 4th Int. Meeting on High Energy Gamma-Ray Astronomy, ed. F. A. Aharonian, W. Hofmann, & F. Rieger (Melville, NY: AIP), 657
Ladouceur, Y., & Pineault, S. 2008, A&A, 490, 197
Lande, J., Ackermann, M., Allafort, A., et al. 2012, ApJ, 756, 5
Landecker, T. L., Roger, R. S., & Higgs, L. A. 1980, A&AS, 39, 133
Lozinskaya, T. A., Pravdikova, V. V., & Finoguenov, A. V. 2000, AstL, 26, 77
Mavromatakis, F. 2003, A&A, 408, 237
Perkins, J. S., Maier, G., Aliu, E., et al. 2009, in 2009 Fermi Symposium, Washington, DC, ed. W. N. Johnson & D. J. Thompson, eConf C0911022, arXiv:0912.3841
Taylor, A. R., Gibson, S. J., Peracaula, M., et al. 2003, AJ, 125, 3145
Trepl, L., Hui, C. Y., Cheng, K. S., et al. 2010, MNRAS, 405, 1339
Uchiyama, Y., Takahashi, T., Aharonian, F. A., & Mattox, J. R. 2002, ApJ, 571, 866
Weinstein, A., Aliu, E., Arlen, T., et al. 2009, in Fermi Symposium, Washington, DC, ed. W. N. Johnson & D. J. Thompson, eConf C0911022, arXiv:0912.4492
Weinstein, A., Aliu, E., Arlen, T., et al. 2011, in Proc. 32nd Int. Cosmic Ray Conf., Vol. 7, 162
Weisskopf, M. C., Swartz, D. A., Carramiñana, A., et al. 2006, ApJ, 652, 387
Zhang, X., Zheng, Y., Landecker, T. L., & Higgs, L. A. 1997, A&A, 324, 641